The Effect of Oxygen Induced Degradation on Charge Carrier Dynamics in P3HT:PCBM and Si-PCPDTBT:PCBMThin Films and Solar Cells

*Safakath Karuthedath, Tobias Sauermann, Hans-Joachim Egelhaaf, Reinhold Wannemacher, C.J. Brabec, Larry L. Lüer**

Optical Spectroscopy and Microscopy of Nanostructured Materials, IMDEA Nanociencia, C/ Faraday, 9, 28049 Cantoblanco (Madrid), Spain.

Belectric OPV GmbH , Landgrabenstr. 94, 90443 Nürnberg, Germany.

Bavarian Center for Applied Energy Research, Fürther Str. 250, 90249 Nürnberg, Germany

4i-MEET, Friedrich-Alexander University, Martensstr. 5, 91058 Erlangen, Germany

SUPPORTING INFORMATION:

Table of contents:

A Derivation of the fitting function for charge decay in degraded samples

Degradation can cause a background of space charges that persist even in the absence of irradiation, by introducing deep traps for one carrier type. These background carriers do not give rise to a transient absorption (TA) signal (because they are not photoinduced), but they do influence the decay kinetics of the photoinduced polarons, because they contribute to recombination.

We assume degradation-induced defects in the donor (P3HT or Si-PCPDTBT) phase that act as acceptors for electrons.[1] The autodissociation equilibrium, given by the dissociation and recombination coefficients k_d and k_a, respectively, cause an excess density of positive polarons that, upon photoexcitation of negative and positive polarons, causes a deviation of polaron recombination kinetics from simple bimolecular behavior. The kinetic scheme is given by

$$\begin{bmatrix} 0 \underset{k_L}{\overset{g(L)}{\rightleftharpoons}} p + n \\ A \underset{k_a}{\overset{k_d}{\rightleftharpoons}} A^- + p \end{bmatrix}, \tag{S1}$$

where 0 signifies a neutral polymer strand, p and n are negative polarons in the donor and acceptor phase, respectively, A and A^- are neutral and negatively charged defects in the donor phase. The generation term g(L) in our experimental setup is a boxcar function that depends on light intensity L. Since the density of negative polarons in the donor phase can be neglected, an interaction between these latter species and A can be neglected. Electro-neutrality then requires that at all times,

$$A^- + n = p \tag{S2}$$

Assuming complete ionization of defect sites, we get $A^- = const = A_{tot}$ (A_{tot} being the total density of degradation-induced defect sites) and therefore

$$p(t) = n(t) + A_{tot} \tag{S3}$$

For eq. S3 to hold during the experimentally accessible time range, we also require the autoionization equilibrium to be faster than the typical recombination times, i.e. in S1, $k_d + k_a \gg k_L n(t)$. This assumption is different from the one by Seemann et.al [1]., who assume that k_a is very slow and thermally activated, which is justified in their system by the observation of a photo-induced build-up of persistent background carriers. Here, we do not

[1]The assumption of electron donors would lead to the same concentration-time law for P3HT polarons, under the given assumptions.

observe such a phenomenon, and we are concerned with an unknown electrochemistry (i.e. we do not know the redox potentials of the irreversible photoinduced defects while Seemann et al, studying reversible oxygen effects, can rely on the known redox potential of the O_2/O_2^- system).

The rate equation for negative polarons is thus given by

$$\frac{dn}{dt} = G(L) - k_L(t) \cdot \left(n(t) + A_{tot}\right) \cdot n(t) \tag{S4}$$

In order to account for dispersive effects, we choose a polynomial ansatz for the recombination coefficient:

$$k_L(t) = k_L^0 \cdot t^{-\gamma} \tag{S5}$$

The experimentally obtained differential absorption ΔA(t), is related to the polaron concentration via the Beer-Lambert law,

$$\Delta A(t) = A(t)_{pumpon} - A(t)_{pump\ off} = \sigma_p^{970\ nm} \cdot \Delta p(t) \cdot d, \tag{S6}$$

Where $\sigma_p^{970\ nm}$ is the positive polaron absorption cross-section at the probe wavelength of 970 nm, d is the film thickness, and Δp(t) is given by

$$\Delta p(t) = p(t)p_{pumpon} - p(t)_{pump\ off} \tag{S7}$$

When the pump pulse is off, n(t) = 0; from S3 we then obtain

$$p(t)_{pumpoff} = A_{tot} \tag{S8}$$

Inserting S3 and S8 into S7, we obtain

$$\Delta p(t) = n(t), \tag{S9}$$

And inserting S9 into S6 and rearranging gives

$$n(t) = \Delta A(t) / \left(\sigma_p^{970\ nm} \cdot d\right) \tag{S10}$$

We insert S10 into S4 and obtain after rearranging

$$\frac{d\Delta A(t)}{dt} = \sigma_p^{970\,nm} \cdot d \cdot g(L) - \frac{k_L(t)}{\left(\sigma_p^{970\,nm} \cdot d\right)} \cdot \left[\Delta A(t) + \sigma_p^{970\,nm} \cdot d \cdot A_{tot}\right] \cdot \Delta A(t) \quad \text{(S11)}$$

We define a spectroscopic recombination rate constant $k_r'(t) = \frac{k_r(t)}{\left(\sigma_p^{970\,nm} \cdot d\right)}$ and a spectroscopic generation term $G'(L) = \sigma_p^{970\,nm} \cdot d \cdot g(L)$. From S6 and S8 we learn that the absorption caused by the "background polarons" is $A_P^{background} = \sigma_p^{970\,nm} \cdot d \cdot A_{tot}$. Inserting these relations into S11, we obtain finally

$$\frac{d\Delta A(t)}{dt} = G'(L) - k_r'(t) \cdot \left[\Delta A(t) + A_p^{background}\right] \cdot \Delta A(t) \quad \text{(S12)}$$

Equation S12 is solved numerically by standard ODE (ordinary differential equation) solvers. By variation of $G'(L)$, $k_r'(t)$, and $A_p^{background}$, we fit the calculated transient absorption profile to the experimental one. For each sample and degradation level, we fit all measured dynamics at different light intensities globally. Minimizing the global error squared with standard non-linear optimization techniques, checking that no systematic deviations are present, and using $\sigma_p^{970\,nm} \approx 10^{-16} cm^2$ for P3HT and $\sigma_p^{970\,nm} \approx 3 \cdot 10^{-17} cm^2$ for Si-PCPDTBT, and d=250 nm, we obtain the device parameters $k_r(t)$ and A_{tot} quantitatively at each degradation level.

In eq. S12, the fitting parameters $A_p^{background}$ and γ (inside $k_L(t)$) both act on the long term asymptotic form of the concentration-time dependence. This raises the question how strong the cross talk between these parameters is expected to be in the fits. Below, we give some simulations that show quite distinct long-time behaviors for variation of γ and $A_P^{background}$, respectively.

In Fig. S1a, both γ=0 and $A_p^{background} = 0$. In this case, eq. S12 has the following solution:

$$\Delta A(t) = \left[{}^{1}/_{A(0)} + k_L t\right]^{-1}, \quad \text{(S13)}$$

which has an intensity independent long-time asymptote of $\Delta A(t) = [k_L t]^{-1}$, which is the same for all starting concentrations and has a slope of -1 in a double logarithmic representation. In Fig. S1b, we leave $A_p^{background} = 0$ but set $\gamma = 0.3$. As can easily be shown, the long-time asymptote is still linear in a double logarithmic representation and independent of the starting concentration, but the slope is now $1 - \gamma = 0.7$. Finally, in Fig.S1c, we set $\gamma = 0$ and $A_p^{background} = 10^{-5}$. In this case, an entirely different long-time solution is obtained: At a time when $A_p^{background}$ becomes comparable to the remaining polaron absorption $\Delta A(t)$, the decay trace deviates from bimolecular recombination. After very long times, $A_p^{background} >> \Delta A(t)$, so the bracket in S12 becomes a constant, and the solution is a stretched exponential. As can be seen in Fig. S1c, such a stretched exponential does not have a linear long-time asymptote, instead it bends towards infinite slope in a double logarithmic representation, nor is the long-term behavior intensity independent: for long times, all curves in Fig. S1c are y-shifted replicas of each other meaning that they deviate by a constant factor. In Fig. S1d finally, $A_p^{background} = 10^{-6}$. The condition $A_p^{background} >> \Delta A(t)$ is now obtained at a much later time than in Fig. S1c. For this reason, the two regimes (linear slope and final stretched exponential) can both be observed separately, at least at high intensities. When the stretched exponential part sets in after the intensity independent asymptote of the bimolecular decay has already been reached, it follows that also all stretched exponentials are independent of the initial concentration. The amount of intensity dependence still present in the stretched exponential part is therefore a probe for the background carrier concentration. Therefore, a global fitting of various curves at different starting concentrations, as performed here, is mandatory to disentangle γ from $A_p^{background}$.

Summarizing this curve discussion, a variation of γ causes a change in the slope of the linear asymptote, while a change in $A_p^{background}$ changes the time at which $A_p^{background}$ and $\Delta A(t)$ become comparable, which results in a deviation from the straight line behavior and in turn

controls how much of the initial intensity variation is still visible in the long time exponential decay phase. These phenomena are well distinguished and therefore both $A_p^{background}$ and γ can be fitted at the same time with low cross talk, ***but only if several curves of different starting concentration are fitted at the same time.*** This justifies the procedure we adopted for the analysis of the charge dynamics in Fig. 3, main manuscript.

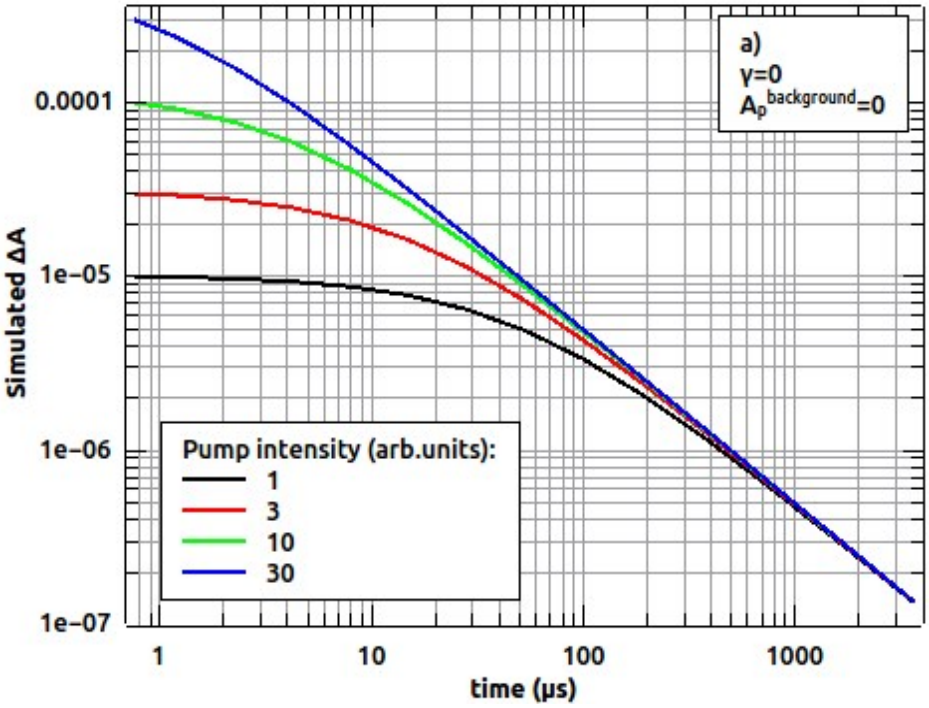

Figure S1.a

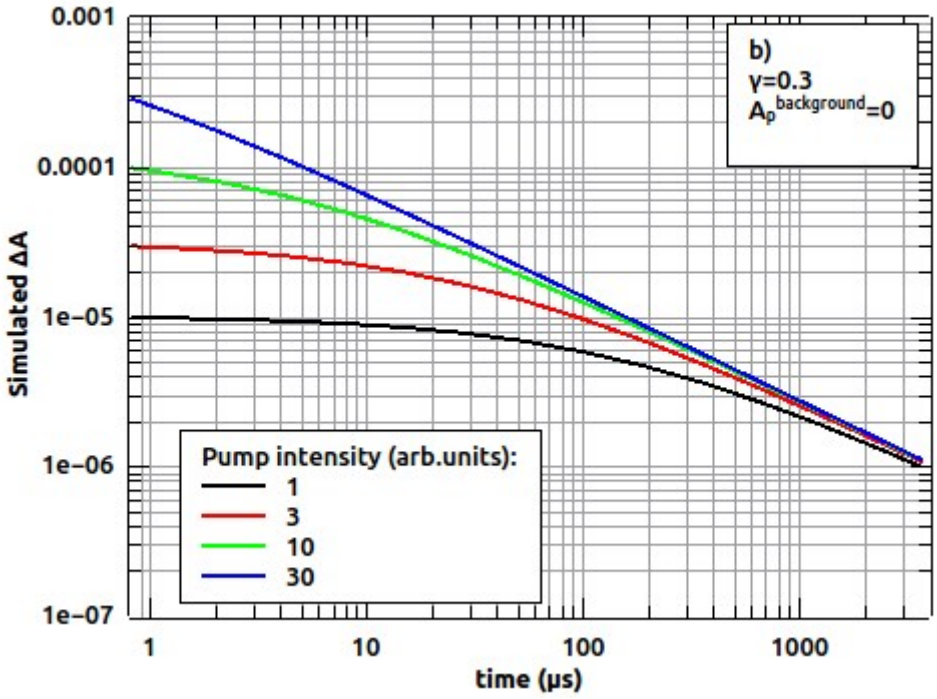

Figure S1.b

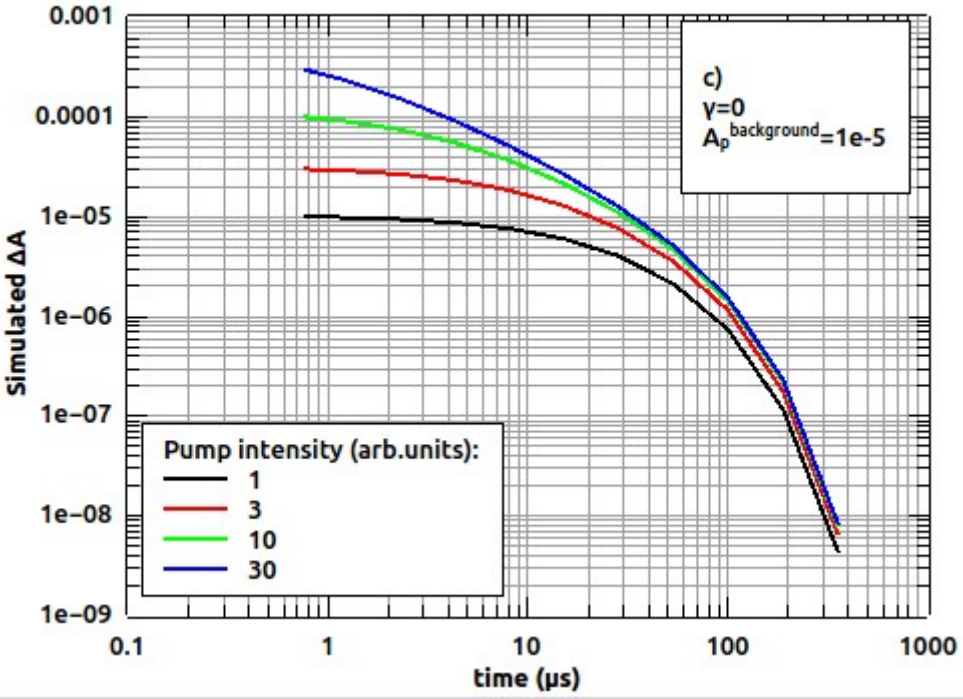

Figure S1.c

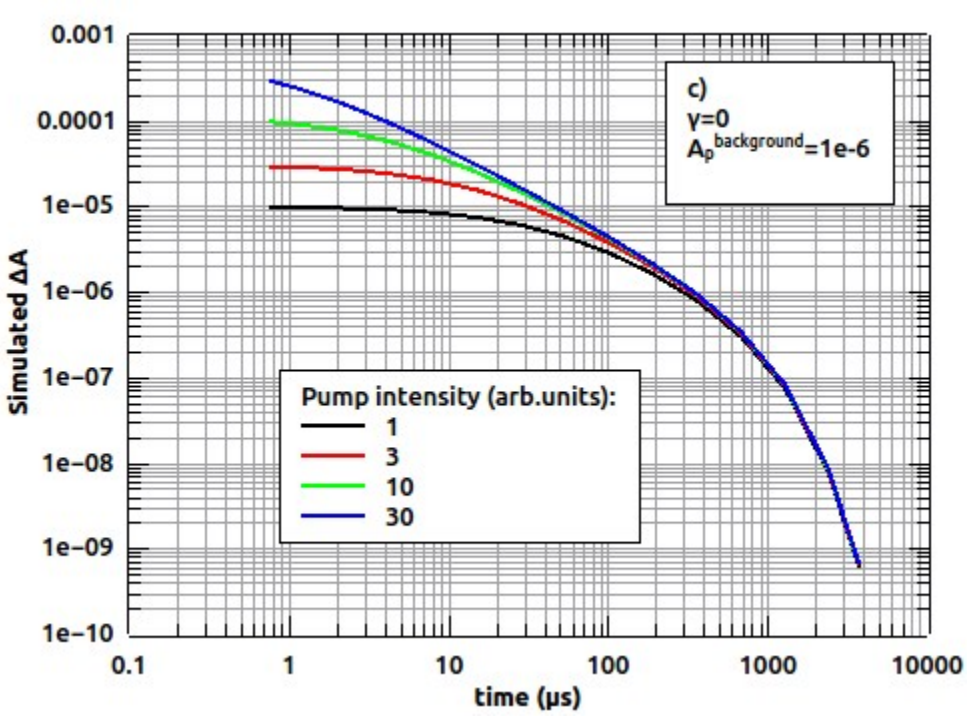

Figure S1.d

B A CLOSER LOOK AT THE GENERATION FACTOR G

G in S12 and S1 (and in eq. 1 and 5 in the main text) is the rate of generation of free charges. It is proportional to the incident photon flux per area and film thickness, the proportionality constant being the yield for photon absorption, exciton dissociation and charge separation:

$$G = J_{ph}/d \cdot \varphi_{abs} \cdot \varphi_{diss} \cdot \varphi_{sep}, \quad \text{(S14)}$$

It is convenient to summarize the yields for absorption, exciton dissociation and charge separation into the generation term, because these processes – and also their counter players photon scattering, exciton deactivation, and geminate recombination, respectively - all occur on the femto to picosecond time scale and therefore do not contribute to the microsecond kinetics. In S14, J_{ph} is the photon flux in cm^{-2}, d (in cm) is the film thickness, φ_{abs} is the absorption probability in the film (φ_{abs} = 0.93 in P3HT as the penetration depth at the

pumping wavelength of 532 nm is much smaller than the film thickness, while in Si-PCPDTBT:PCBM, it is only about 10%) and φ_{sep} is the charge separation probability after a photon has been absorbed. We do not need to consider the inhomogeneity of polaron generation along the depth axis due to the finite light penetration depth for wavelengths of strong absorption, because charge carrier diffusion through the film thickness occurs on a time scale faster than our experiment. Effects such as exciton annihilation or picosecond charge recombination can be safely excluded by using weak continuous wave lasers as in the present case.

Since the external quantum efficiency, EQE, is given by:

$$EQE = \varphi_{abs} \cdot \varphi_{diss} \cdot \varphi_{sep} \cdot \varphi_{extr}, \quad \text{(S15)}$$

we can insert S15 into S14 yielding:

$$EQE/\varphi_{extr} = Gd/J_{ph} \quad \text{(S16)}$$

We can call the term EQE/φ_{extr} the ***free polaron yield*** (i.e. polarons that survived geminate recombination relative to absorbed photons).

We used S14 to fit the "on" curves under illumination In Fig. 2, and then S16 to calculate the free polaron yield (see Fig. 4a, black symbols) from the fitting parameter G and the pump intensity. In the fitting, we noted a strong interdependence between k_r, γ and c_b, both γ and cb tending towards zero. This can be understood by the fact that in Fig.2, continuous illumination has been used. Most of the data points are within 50% from the maximum, so that μ does not vary much and hence γ is close to zero. For the same reason, c_b cannot be fitted accurately because the effect of background carriers is only seen at low carrier concentrations, of which

we have only 2 reasonable data points in Fig.2. For this reason, we fixed both γ and c_b to zero in the fitting of G. The results are displayed in Fig. 4a for P3HT:PCBM at various degradation levels, showing no significant change of G under increased degradation.

C Femtosecond transient absorption in Si-PCPDTBT

Femtosecond transient absorption (TA) spectroscopy is used to trace photophysics that occur on a time scale of femto to picoseconds. In organic photovoltaics, exciton dissociation and geminate recombination, prominent loss processes that reduce the generation yield, have been shown to occur on this time scale. In contrast to microsecond TA, where essentially only one type of photoexctation (positive polarons in the donor phase) is visible, in femtosecond TA we additionally observe neutral singlet excitons. The TA spectra of singlets and polarons generally overlap, so matrix decomposition techniques need to be used to obtain the time-resolved population of singlet excitons and polarons separately. We follow a procedure called target analysis described by van Stokkum et al[2].

In short, we apply Beer-Lambert's Law,

$$A(t,w) = \sum_i c_i(t)\sigma_i(w) \tag{S17}$$

to reproduce the measured transient absorption spectrum A(t,w), which depends on time t and probe energy w, by a superposition of states I with characteristic time-resolved concentration $c_i(t)$ and energy-resolved absorption cross-section σ(w). Eq. S17 can be written in matrix form:

$$A = c \times \sigma \tag{S18}$$

In eq. S18, each column of the c matrix represents one complete concentration-time dependence of a state i, while each row of the σ matrix represents the full (time-invariant) spectrum of that state i. Of course, any linear combination E of the spectra in the σ matrix

$$E = s \times \sigma, \tag{S19}$$

S being the spectral weight matrix, can also solve eq. S18, as can be seen by introducing S19 into S18:

$$A = c \times s^{-1} \times E \tag{S20}$$

and substituting $c \times s^{-1} \equiv c'$:

$$A = c' \times E \tag{S21}$$

The concentration-time matrix c_{SEQ} of a strictly sequential reaction $0 \rightarrow S_1 \rightarrow S_2 \rightarrow S_3 \rightarrow 0$ (no back reactions, no parallel reactions, no parallel generation of the excited states S_i from the ground state 0) is analytically known [2]. Hence, assuming a strictly sequential reaction, we can find the E matrix by simply multiplying the inverted c_{SEQ} with the measured TA spectrum:

$$E = (c_{SEQ})^{-1} \times A \tag{S22}$$

In case the assumption of a strictly sequential reaction path happens to be right, then $c = c_{SEQ}$ from which immediately follows $E = \sigma$. In this simple case, evaluation of S22 directly yields the spectra of the photophysical states $\sigma_i(w)$. Generally, however, photophysical reaction paths are not strictly sequential. In organic photovoltaics, it has been shown that part of the polaron generation occurs on a time scale < 100fs, and thus in parallel with singlet generation. Singlets can sequentially convert into polarons, but in parallel they can directly decay to the ground state by some ultrafast mechanisms (exciton annihilation, ultrafast deactivation of

short-lived charge transfer state between donor and acceptor). If we apply S22 in this general case, then the resulting matrix E will not directly represent the spectra of the photophysical states, but superpositions of these, according to S19.The rows in E are therefore called ***evolution-associated differential spectra (EADS)*****,** while the rows in the σ matrix are called **species-associated differential spectra (SADS).** In order to solve S19, the spectral weight matrix s must be found using additional photophysical knowledge. This is done by designing a test matrix σ_{test}, consisting of a spectral model for all contributing excited states, satisfying existing photophysical knowledge but providing some adjustable parameters. Using the standard Levenberg-Marquardt optimization technique, we minimize the error between the E matrix obtained from S19 and the one obtained from S22, by varying the free parameters in σ_{test}. In doing so, we obtain also the spectral weight matrix s, which we can use to go from the sequential concentration matrix to the actual one. In the last step, the concentration matrix is fitted to a target model containing all possible reaction paths and associated rate constants. In our case, this last step is not necessary. Since we are interested in the polaron yield per absorbed photon, we can get this information directly from the spectral weight matrix.

To illustrate the above procedure, we present below the single steps for obtaining the polaron yield in pristine Si-PCPDTBT. First we apply eq. S22 to find the E matrix that best reproduces our measured TA spectrum, which is given on the left in fig. S2. We do this by non-linear optimization of the exponential lifetimes in the sequential concentration matrix c_{SEQ}, by minimizing the error between the calculated A (using eq.21) and the measured one. The quality of the fit is shown in Fig. S2, right: all dynamic features are nicely reproduced, namely (i) a fast decay of photoinduced absorption (PA) around 0.9 eV, (ii) a fast build-up of PA around 1.4 eV, and (iii) a fairly constant photobleach (PB) around 1.6 eV.

Fig. S3 shows the EADS (rows of the E matrix), that can be used in eq. S21 to calculate the reproduced TA spectrum (Fig. S3 right) after building the c' matrix with the lifetimes of the EADS, given in the inset.

The second step is to apply S19 to fit the EADS by a superposition (with relative weights in matrix s) of the spectra of the photoexcitations in matrix σ. We assume only 2 photoexcitations: singlet excitons and polarons. Since both these photoexcitations involve the electronic system of Si-PCPDTBT, they share the same photobleach (PB). Irrespective whether a polaron or a singlet exciton is formed on a conjugated segment of Si-PCPDTBT, the bleach it creates is always the same. The spectral weights that we obtain, are therefore directly proportional to the concentration of the species.

As shown in Fig. S4, the spectrum of the singlet exciton involves, apart from the PB features at 1.7 and 1.9 eV, a PA band at 0.87 eV with vibronic replicas at 1.04 and 1.2 eV, a stimulated emission band at 1.34 eV, and a higher energetic PA band at 2.55 eV. The polaron spectrum contains, apart from PB, a PA at 1.03 eV followed by vibronic replicas at 1.18 and 1.34 eV, and a broad PA at 2.3 eV. Multiplying these spectra with the spectral weights that are given in the inset of Fig.S4, yields the thick lines in Fig. S3, showing near perfect agreement with the EADS spectra (thin lines). The spectral weights can therefore be considered reliable.

Finally, the polaron yield at 100 ps is obtained by using the inset of Fig. S4 to divide the polaron spectral weight in EADS2 by the sum of the singlet and polaron spectral weights in EADS0. This procedure yields the first blue symbol in Figure 4a, main manuscript, for 0% JSC loss. Then the whole procedure is repeated with analogous TA spectra of the degraded samples.

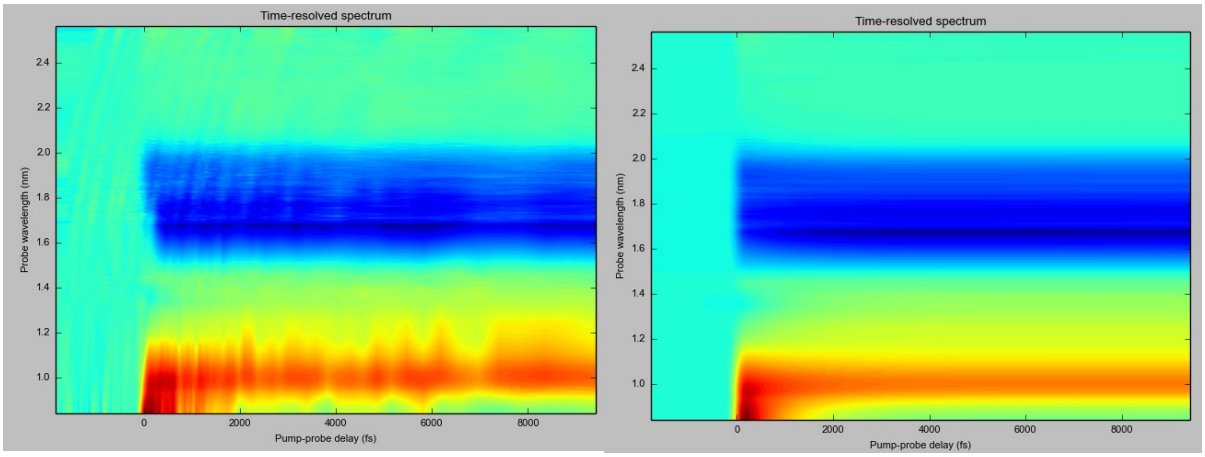

Figure. S2: (left) TA spectrum of pristine Si-PCPDTBT after pumping at 390 nm with 150 fs, 10 nJ pulses of 300 μm spot size; (right) global fit using eq. S22.

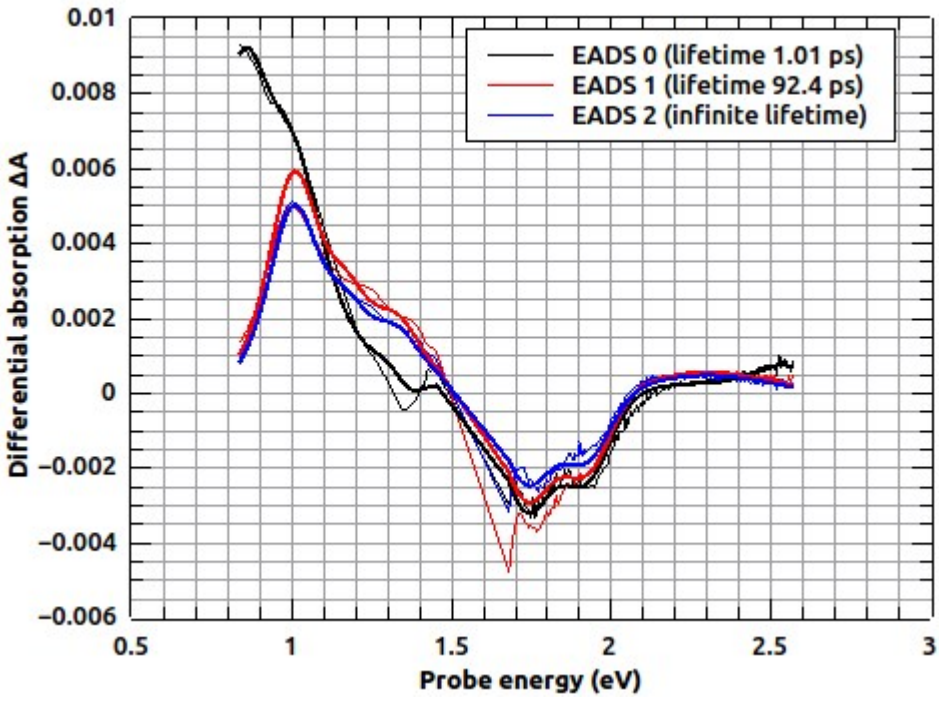

Figure. S3: EADS (rows of E matrix) and associated lifetimes(thin lines). Thick lines: EADS reproduced using eq. S19 with the SADS (σ matrix) and spectral weights as shown below.

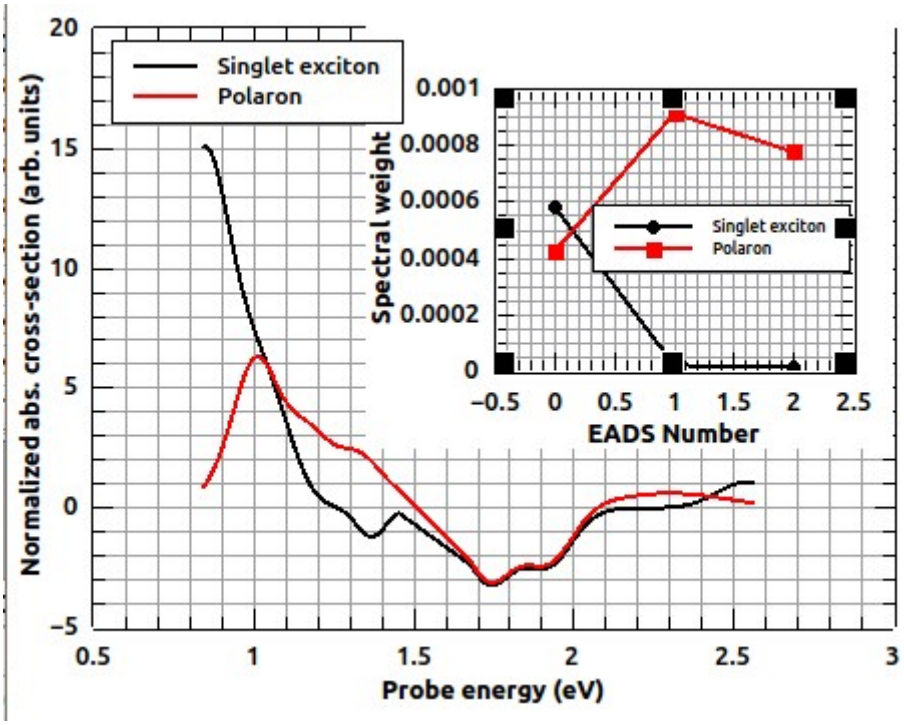

Figure. S4: SADS (rows of the σ matrix) and corresponding spectral weights to reproduce the EADS in Fig. S3

D FEMTOSECOND SPECTROSCOPY IN P3HT:PCBM FILMS

EADS spectra for P3HT:PCBM films were obtained in the same way as described above for Si-PCPDTBT. An analogous treatment to obtain specific spectral weights for polarons and singlets is however complicated by the presence of two donor phases (amorphous and ordered), each with distinct optical probes for singlets, polarons and the corresponding bleach. A target analysis of P3HT:PCBM films will be the focus of a forthcoming publication. Here, we follow the simplified treatment of Guo et al [3] who obtained specific kinetics for singlet and charged states by subtracting the singlet contribution to the charge transient at 1.24 eV, which they found to be about one third of the maximum of the singlet absorption band at 1.0 eV, which is pure because there is no oscillator strength for the charge absorption band at that probe energy. Applying this procedure to our EADS yields spectral weights of the singlet and polaron bands, however with unknown relative cross-sections because the optical probes for

P3HT polarons and singlets are not locked via the common PB signal as in our treatment of the Si-PCPDTBT data. Therefore, applying Guo's treatment cannot yield the absolute polaron yield, as our target analysis can, but only a quantity which is proportional to it. In order to trace degradation effects, a quantity which is proportional to the known pristine IQE is however sufficient. In Fig. 4a of the main manuscript, we therefore scaled the polaron yields from the EADS (red symbols) to match the black symbol for the pristine sample. It is found that the polaron yields for the degraded sample do not show a significant dependence on degradation, in agreement with the microsecond data which are absolute.

E Absorption spectra

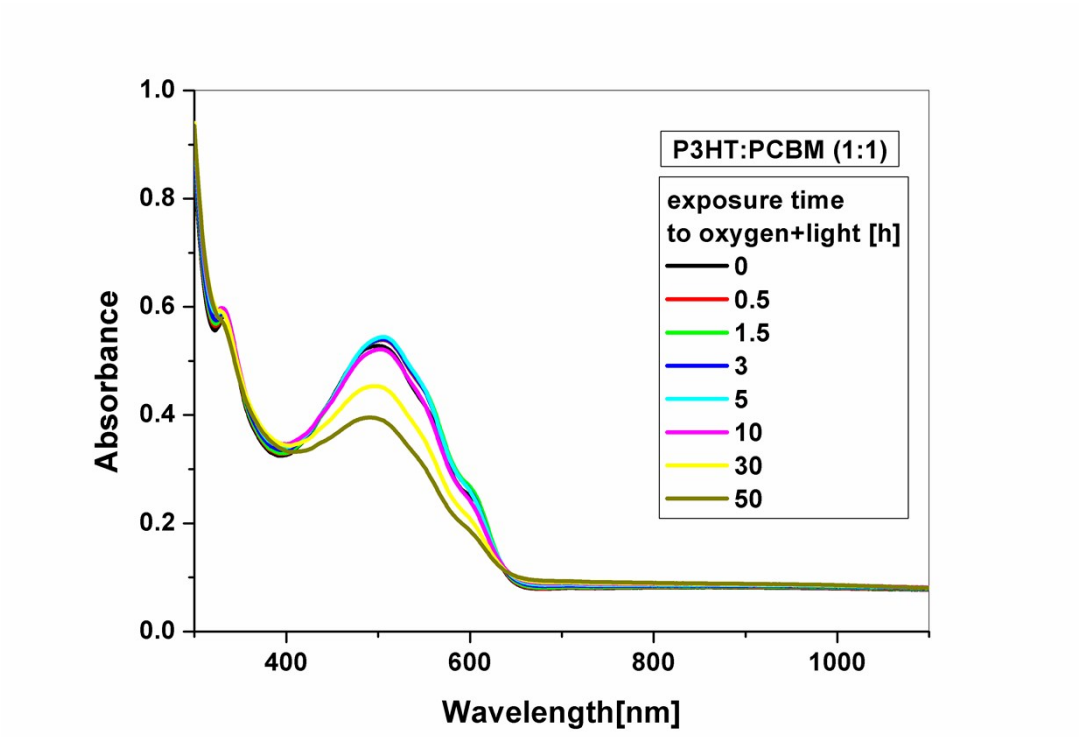

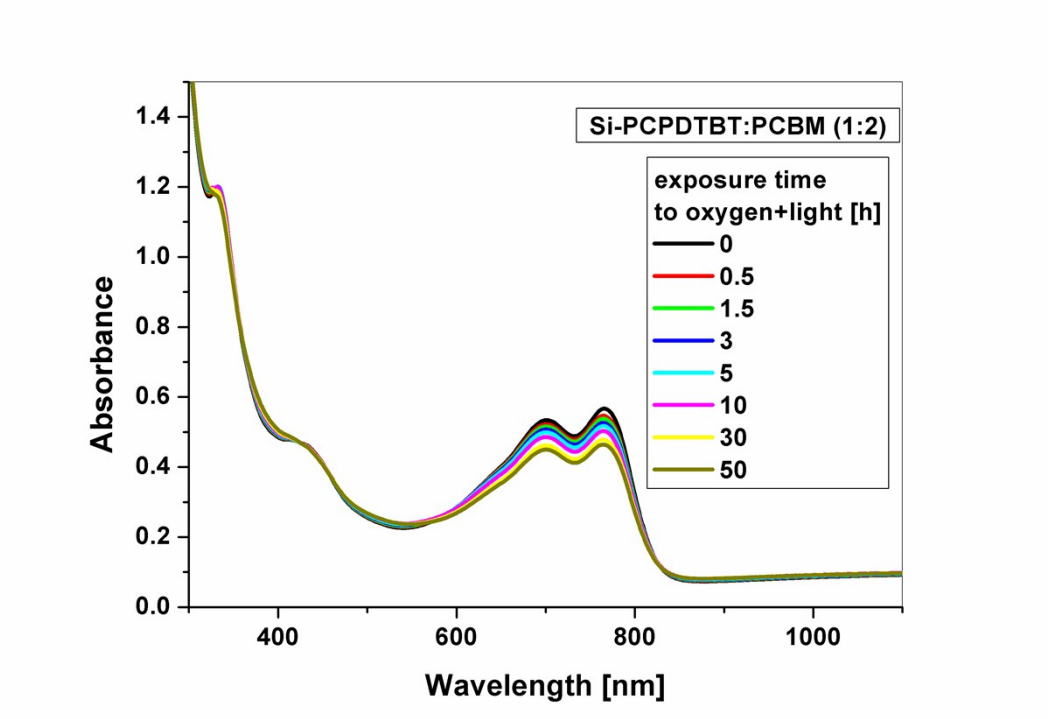

F Pulsed TA measurements

Pulsed transient absorption measurements were performed with a 532nm laser with 300 picosecond pulses.

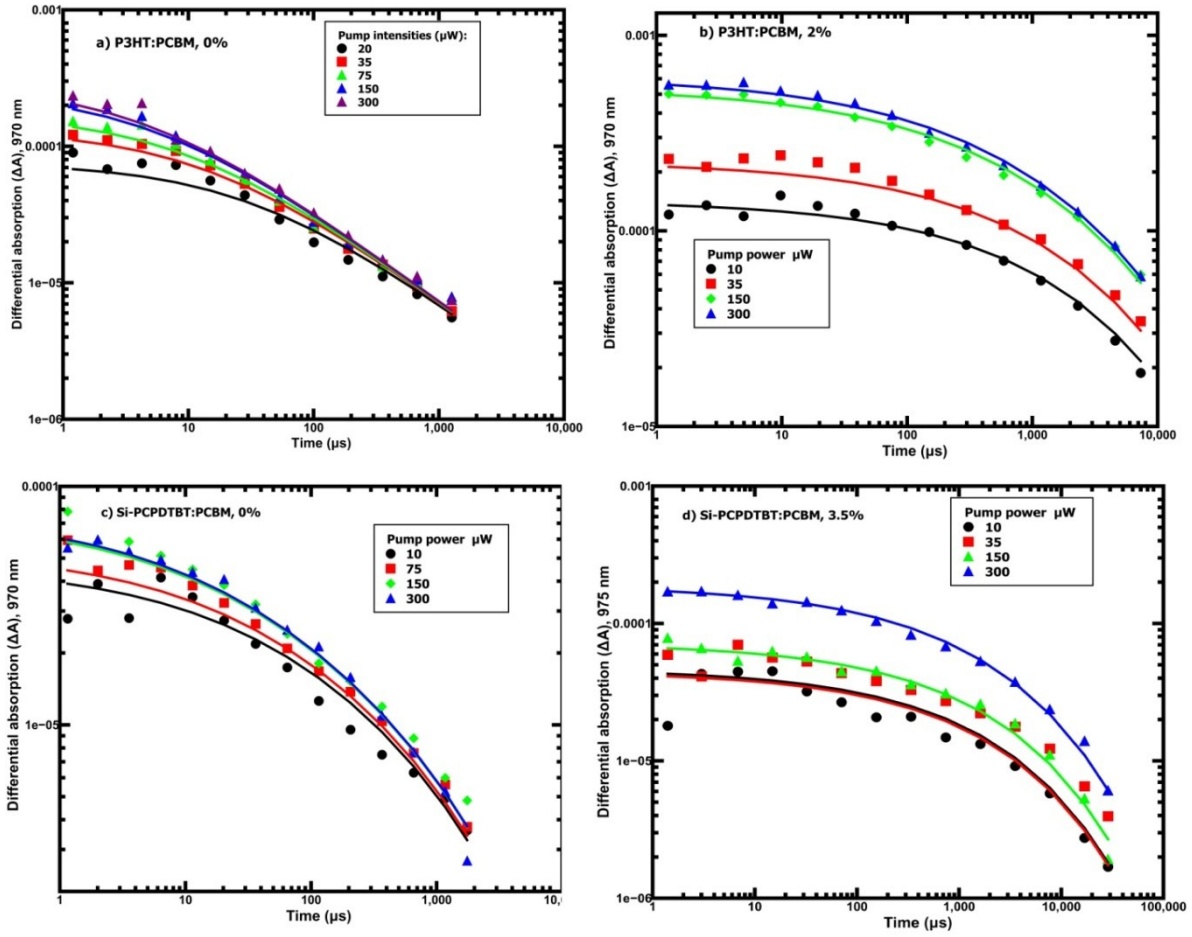

LITERATURE:

[1] A. Seemann, T. Sauermann, C. Lungenschmied, O. Armbruster, S. Bauer, H.-J. Egelhaaf, J. Hauch, *Solar Energy*,**2010**, 85, 1238.

[2] Ivo H.M. van Stokkum *, Delmar S. Larsen, Rienk van Grondelle, *Biochimica et Biophysica Acta*, **2004**, 1657, 82 – 104

[3] J. Guo, H. Ohkita, H. Benten, S. Ito, *J. Am. Chem. Soc*. **2010**,132, 6154.